Received: 21 March 2018 | Revised: 6 June 2018 | Accepted: 13 June 2018

DOI: 10.1002/rcm.8214

RESEARCH ARTICLE

WILEY Rapid Communications in Mass Spectrometry

Dating igneous rocks using the Potassium–Argon Laser Experiment (KArLE) instrument: A case study for ~380 Ma basaltic rocks

Yuichiro Cho[1,2] | Barbara A. Cohen[1]

[1] NASA Goddard Space Flight Center, 8800 Greenbelt Rd, Greenbelt, MD 20771, USA

[2] University of Maryland Baltimore County, 1000 Hilltop Circle, Baltimore, MD 21250, USA

Correspondence
Y. Cho, NASA Goddard Space Flight Center, 8800 Greenbelt Rd, Greenbelt, MD 20771 USA.
Email: yuichiro.cho@nasa.gov

Funding information
Japan Society for the Promotion of Science, Postdoctoral Fellowship for Research Abroad

Rationale: We report new K–Ar isochron data for two ~380 Ma basaltic rocks, using an updated version of the Potassium–Argon Laser Experiment (KArLE), which is being developed for future *in situ* dating of planetary materials. These basalts have K contents comparable with those of lunar KREEP basalts or igneous lithologies found by Mars rovers, whereas previous proof-of-concept studies focused primarily on more K-rich rocks. We aim to measure these analogous samples to show the advancing capability of *in situ* K–Ar geochronology.

Methods: Combining laser-induced breakdown spectroscopy (LIBS), mass spectrometry (MS), and microscopic analyses, we measured the abundance of K and ^{40}Ar from 23 spots on the basalt samples. We then constructed K–Ar isochron plots from these rocks. The breadboard instrument consists of flight-equivalent devices including a 30-mJ Nd:YAG laser and a quadrupole mass spectrometer.

Results: Despite much lower K abundances than in previous studies, the isochron slopes yielded 380 ± 44 Ma and 398 ± 50 Ma for 380.7-Ma and 373.5-Ma rocks, respectively, indicating that accuracy better than 25 Ma (<7%) is achievable with our instrument. The isochron intercepts both yielded trapped ^{40}Ar approximately 1×10^{-6} cm^3 STP/g.

Conclusions: Our experimental results demonstrate that accurate and precise measurements are possible using the KArLE approach on basaltic rocks, which are ubiquitous on planetary surfaces, and are useful in addressing a wide range of questions in planetary science.

1 | INTRODUCTION

Geochronology is a fundamental tool to understanding the history of planetary and asteroidal bodies. Radiogenic ages of rocks provide the absolute timing of geological events as well as the duration of geochemical or climatic conditions prevailing in the planetary/asteroidal body. Dating rocks from multiple horizons by a rover travelling on the planet or multiple landers at different sites further allows the entire history of the planet to be reconstructed. Such measurements will enable us to place the history of individual planetary bodies into the context of the entire solar system evolution. The capability of *in situ* geochronology on board planetary landers or rovers is highly desirable given the challenges and highly limited opportunities for sample return missions.[1]

Three geochronology experiments have been conducted on Mars using the Curiosity rover.[2-4] These experiments demonstrated the feasibility of *in situ* K–Ar dating on Mars and underlined the utility of acquiring absolute ages along with other geochemical data, such as elemental and mineralogic composition of rocks. However, the results also revealed challenges involved with this technique, such as the difficulty in extracting ^{40}Ar from highly retentive minerals using the onboard furnace,[4] the incapability of directly measuring the mass of the sample,[2] and the possibility of mineral sorting/separation during the sample delivery.[4]

To resolve these problems and expand the capability of *in situ* geochronology, several groups, including ours, have been developing K–Ar dating instruments based on a laser-ablation approach.[1,5-12] In this technique, laser pulses vaporize the sample surface, liberating K and Ar locally (hundreds of microns in diameter and depth). The concentrations of K and ^{40}Ar in the laser spots are measured with laser-induced breakdown spectroscopy (LIBS) and mass spectrometry (MS), respectively (LIBS–MS approach). The LIBS–MS approach is attractive for flight implementation because its components (laser, optical spectrometers, mass spectrometer and micro-imaging) have flown on multiple missions, including aboard Curiosity as ChemCam, SAM, and MAHLI, respectively. This feature is advantageous because building on this flight heritage reduces the cost, time, and risk of hardware development. The K–Ar Laser Experiment, KArLE, implements the LIBS–MS approach using components with performance characteristics similar to flight.[1]

Several proof-of-concept studies have shown that the LIBS–MS analysis of heterogeneous rocks allows isochrons to be constructed and radiogenic ^{40}Ar to be discriminated from trapped ^{40}Ar.[1,10]

The applicability of the performance analysis conducted by these studies, however, could be limited because of the insufficient fidelity of the measured samples and their experimental setups. First, the terrestrial rocks measured in previous studies were very K-rich, coarse-grained, and/or heterogeneous, such as a granite, a K-rich tuff,[1] or gneiss.[10] As a result, the K–Ar isochrons largely relied on data points measured in biotites or K-feldspars, which contain very high (>5 wt%) K. Although such rocks are favorable for K–Ar isochron dating, the majority of planetary surfaces are covered with basaltic rocks,[13,14] which are typically much K-poorer and much more homogeneous. Thus, the capability of isochron measurements could be limited when more homogeneous, K-poor rocks are measured in actual missions. In fact, more than 50% of ChemCam data exhibit K_2O abundance less than ~6500 ppm, while only <25% samples show K_2O abundances higher than 3 wt%.[15] Thus, the capability of the LIBS–MS approach needs to be assessed for basaltic rocks to further validate its performance as an *in situ* dating technique.

Second, using components and experimental conditions different from those achievable on landed missions hinders a reliable assessment of actual performance of the geochronology experiments. For example, Cho et al[10] used a high-energy (100 mJ) laser, a cold trap cooled with liquid nitrogen, and a Ti–Zr getter heated to a high temperature (700–800°C). The same concern holds for an innovative LIBS–MS study using a quadrupled ultraviolet (UV) Nd:YAG laser;[11] although a 170-Ma basaltic rock was measured, the laser-ablation process depends on the wavelength of laser emission, and only the infrared (IR) laser is flight qualified for LIBS at this time. Solé[12] used the known terrestrial ratios of Ar isotopes to correct for trapped Ar in the samples studied, a technique that will not be applicable to the Moon or Mars.

Thus, in this study, we conducted a series of case-study experiments to measure basaltic rocks using an instrument suite and experimental conditions more comparable with flight instruments to investigate the accuracy and precision that KArLE can achieve in a more realistic situation.

2 | EXPERIMENTAL

This study used the breadboard geochronology instrument developed by Cohen et al[1] with some upgrades. Major upgrades include the following: (1) the pulse energy of the Nd:YAG laser was attenuated to 30 mJ to simulate the laser equipped on Curiosity;[16] and (2) the shutter of the optical spectrometer was synchronized with the laser pulses to reduce the dark noise of the optical spectrometer. The shutter opened before the laser pulses generated plasma. The exposure time was set at 1 ms, which is sufficiently longer than the typical timescale of laser-induced plasma under a high vacuum condition (<1 μs),[17] to record the time-integrated emission from the plasma.

Two ~380 Ma basaltic rocks from Viluy traps, Siberia (TL-18 (380.7 ± 5.4 Ma) and TO-35 (373.5 ± 5.3 Ma)[18]) were measured with the KArLE breadboard. The thin section indicates that TL-18 has relatively large plagioclase crystals as long as 1 mm × hundreds of microns, whereas TO-35 is composed of much finer minerals.[18] Both samples were cut into slabs and placed in the analysis chamber. The bulk density of the rocks was measured with an electronic scale to be 2.8 ± 0.2 g/cm^3, which was used for the age calculation. In actual missions, the density of minerals would be measured by combining elemental analysis and porosity assessment using LIBS and an imager, respectively.[1] The concentration of K_2O in plagioclase was 4200 ppm for TL-18 and 6400 ppm for TO-35.[18]

The LIBS–MS data were acquired following the procedure below. After placing both of the samples in the KArLE chamber, the entire vacuum system was pumped down and baked at 150°C for 48 h. The typical background pressure in the vacuum line was of the order of 10^{-7} Pa. We analyzed 13 spots for TL-18 and 10 spots for TO-35. Before measuring each spot, 5 precursory laser shots were applied to remove any gases adsorbed at the surface of the sample. After pumping out the surface-related gases, 500 laser pulses were applied on each spot to generate plasma as well as to extract gas from the sample. The LIBS spectra from the plasma were averaged over 50 shots in the optical spectrometer. We thus acquired 10 spectra per laser pit, which were then averaged to obtain one LIBS spectrum representing each laser spot. A dark spectrum was obtained separately and subtracted from the emission spectrum. The optical spectrometer measured the wavelength range of 723–812 nm with a resolution of 0.2 nm FWHM (full width at half maximum). The pulse energy and the pulse repetition rate were set at 30 mJ and 3 Hz, respectively, to simulate the laser used by ChemCam.[16] The spectral response function was not corrected in this study.

The gas liberated from the samples was then purified for 5 min by a GP-50 getter (SAES Getters, Milan, Italy) heated at 430°C. The purified gas was admitted to a quadrupole mass spectrometer in a static operation (i.e., isolated from the pump). The mass spectrometer recorded the time evolution of the signal intensity at *m/z* 39 and 40 for ~200 s. The integration time was 100 ms for both *m/z* values. The entire data acquisition, from starting laser shots to pumping out measured gas, took approximately 10 min. The volume of the laser-ablation pits was measured externally with a laser microscope (see Cohen et al[1] for details of volume estimation). We did not use a cold trap in this experiment, while Cho et al[10] used one to concentrate ^{40}Ar and to remove hydrocarbons efficiently.

The concentration of K in each laser spot was determined using two calibration curves covering different concentration ranges (Figure 1): a linear function covering K_2O < 1.1 wt% and a quadratic function covering 1.1–3.0 wt% K_2O. Both calibration curves were constructed by measuring K_2O standards and used the sum of the intensities of K emission lines at 766.5 and 769.9 nm (I_K). The intensity of each K emission line was calculated by integrating the area under the peak. The base area of each peak was approximated by a right-angled trapezoid where long and short sides were calculated by averaging the intensities over 10 pixels located right before the shorter wavelength limit or right after the longer wavelength limit used for the peak area integration. Then, the intensities of the emission lines were normalized with the total emission intensity recorded by the optical spectrometer (I_{total}). This normalization reduces the signal variation caused by the inevitable shot-by-shot fluctuation of laser pulse energy, as well as by the variable emission intensity from plasma generated in a laser pit.[19] The normalization with the total emission intensity is equivalent to that with the continuum intensity, a normalization examined by Cho et al,[6] because the majority of the emission intensity derives from continuum emission.

A weighted linear regression procedure was used for the data points showing I_K/I_{total} < 0.01 (corresponding to <1.1 wt%). The weighting was implemented to improve predictive capabilities for low-K samples. The weighting factor was the standard deviation of the signal intensity from the replicate measurements of the reference samples. The calibration data were also regressed with a quadratic equation. This calibration curve was used for the data points showing 0.01 < I_K/I_{total} < 0.02 (i.e., 1.1–3.0 wt%) to address the potential self-absorption effect.[20] We confirmed that the two calibration curves yielded virtually identical K contents in the transitional K concentration range (1.0–1.2 wt%).

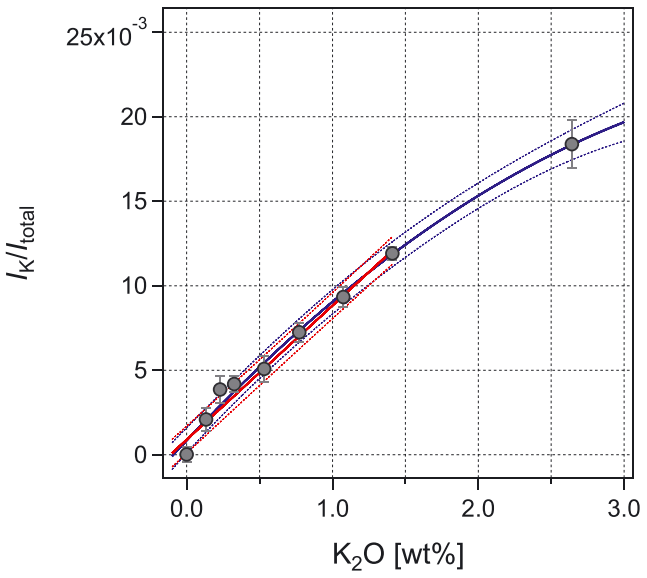

FIGURE 1 Potassium calibration models using standard samples. A linear regression was applied at K_2O < 1.1 wt% and a quadratic curve was used at K_2O > 1.1 wt% to address potential self-absorption effect [Color figure can be viewed at wileyonlinelibrary.com]

The error of K contents was determined based on the width of the prediction band at the intensity ratio measured in each experiment.[6,9] In this study, the amount of error (i.e., the width of the prediction band) was constant at 1000 ppm when the K_2O abundance was below 1.1 wt%, whereas it was larger in the 1.1–3.0 wt% K_2O range. In the latter range, positive errors are always larger than negative errors due to the asymmetrical nature of the prediction band. Here we assigned the larger positive errors as analytical errors of K to conservatively estimate the uncertainties of K abundances.

The detection limit of K_2O was 1000 ppm based on the 1σ prediction band approach, although the K emission line at 766 nm was still detected with a 3σ level from a calibration sample containing 1300 ppm K_2O. The detection limit in this study was higher than that of Cho et al[6] (87 ppm) by an order of magnitude. This can be attributed to the lower quantum efficiency of the optical spectrometer detector used in this study, as well as the smaller number of the standards. Note that the quantum efficiency of the spectrometer used by Cho et al[6] was comparable with that of the ChemCam.[21]

The abundance of ^{40}Ar was measured with the quadrupole mass spectrometer. The sensitivity for Ar measurements in static mode (α) was calibrated in advance by measuring the known amount of terrestrial air using a pipette and a tank. We multiplied this factor by the ion current acquired by the mass spectrometer to calculate the amount of ^{40}Ar released from the samples. We fitted the temporal change of the signals with a linear function and regressed the ion current back to t_0 (i.e., the time when the valve leading to the mass spectrometer opened). A procedural blank was measured before each gas analysis and subtracted from the mass spectrum of the gas.

The detection limit of ^{40}Ar is determined by the amount of background gas. The background level at m/z 40 was 1.4×10^{-11} cm^3 STP on average, gradually decreasing from 2×10^{-11} to 9×10^{-12} cm^3 STP as the experiments proceeded from the first spot of TL-18 to the tenth spot of TO-35. The lowest blank level is comparable with the blank level of 8×10^{-12} cm^3 STP reported by Cho et al[10] using a different experimental setup. The blank levels for other mass numbers were 1×10^{-12} cm^3 STP for m/z 36, 1×10^{-12} cm^3 STP for m/z 38, and 1×10^{-11} cm^3 STP for m/z 39. The presence of hydrocarbons is inferred by the fact that the ratio of the blank at m/z 40 and 36 was ~10, much smaller than the isotopic ratio of Ar in the terrestrial air (i.e., $^{40}Ar/^{36}Ar$ = 298.6).[22]

The gas released from the sample can contain C_3H_4 in addition to ^{40}Ar at m/z 40. Therefore, the isobaric correction was performed following the same procedure employed by the geochronology experiments on Curiosity, using the signal at m/z 39 (C_3H_3) as a tracer.[2] We estimated the abundance ratio of C_3H_4/C_3H_3 using the spots where K was not detected with LIBS, because such data points are expected to contain little to no ^{40}Ar. The estimated contribution from C_3H_4 was subtracted from the signal at m/z 40 using the equation $M_{40Ar} = M_{40} - kM_{39}$, where k = 0.59 ± 0.02 for TL-18 and 0.87 ± 0.04 for TO-35. Here, M_{40} and M_{39} denote the signal intensities at m/z 40 and 39 after blank corrections, respectively. The k values were determined by the lowest M_{40}/M_{39} ratio observed with each sample.

The K–Ar age of the sample t and its error Δt are written as Equations 1 and 2, respectively, using the observables obtained in this study:

$$t = \frac{1}{\lambda}\ln\left(1 + \frac{C\alpha M_{40Ar}}{\rho V[K_2O]}\right) \quad (1)$$

$$\Delta t = \frac{C\alpha M_{40Ar}}{\lambda(\rho V[K_2O] + C\alpha M_{40Ar})}\sqrt{\left(\frac{\Delta[K_2O]}{[K_2O]}\right)^2 + \left(\frac{\Delta\rho}{\rho}\right)^2 + \left(\frac{\Delta V}{V}\right)^2 + \left(\frac{\Delta\alpha}{\alpha}\right)^2 + \left(\frac{\Delta M_{40Ar}}{M_{40Ar}}\right)^2} \quad (2)$$

where

$$M_{40Ar} = (S_{40} - B_{40}) - k(S_{39} - B_{39})$$

$$\Delta M_{40Ar} = \sqrt{(\Delta S_{40})^2 + (\Delta B_{40})^2 + (\Delta k)^2(S_{39} - B_{39})^2 + k^2\left\{(\Delta S_{39})^2 + (\Delta B_{39})^2\right\}}.$$

Here, C is a unit conversion factor. The unit conversion involves constants F_{40K} (naturally occurring fraction of ^{40}K in total K) = 0.01167% and M_K (K atomic mass) = 39.1 g/mol, the molar mass ratio $2M_K/M_{K2O}$ = 0.830, and M_V (the molar volume of a gas at standard temperature and pressure) = 22400 cm^3/mol. λ and λ_e refer to the total and electron-capture decay constants.

$$C = \frac{\lambda}{\lambda_e}\frac{M_K}{\left(\frac{2M_K}{M_{K2O}}\right)F_{40K}M_V} \times 100$$

Here, the uncertainty in K_2O concentration ($[K_2O]$) measured with LIBS is denoted as $\Delta[K_2O]$. The error assigned to the amount of ^{40}Ar was calculated based on the propagation of multiple errors: the uncertainties in the temporal regression of the signals and blanks for the m/z values of 40 and 39, the contribution of the blanks at m/z 39, mass spectrometer sensitivity for Ar analysis in the static mode α, and isobaric correction factor k. Because measuring the concentration of ^{40}Ar ($[^{40}Ar]$) requires the mass of ablated sample, its error involves those in sample density ρ and laser pit volume V. Here, the signals at m/z 40 and 39 are S_{40} and S_{39}, respectively; and the blanks are B_{40} and B_{39}. Their regression errors are denoted as ΔS_{40}, ΔS_{39}, ΔB_{40} and ΔB_{39}. The magnitude of individual errors observed in this study is discussed in the following section.

3 | AGE MEASUREMENT RESULTS AND DISCUSSION

Figures 2 and 3 show examples of LIBS and MS data acquired in this study, respectively. The two examples of the LIBS spectra show the two K emission lines and an O triplet peak overlying the continuum emission. No other obvious peak was observed in the wavelength range of our optical spectrometer.

Figure 3 shows the time evolution of gas abundances at m/z 40 and 39 immediately after the gas was admitted to the quadrupole mass spectrometer, as well as corresponding procedural blanks. The signals at m/z 40 are almost constant over the experiment time (+0.7%/min), as expected for a noble gas. In contrast, those for m/z 39, for example, decrease at a rate of 4%/min, suggesting that they are composed of hydrocarbons.

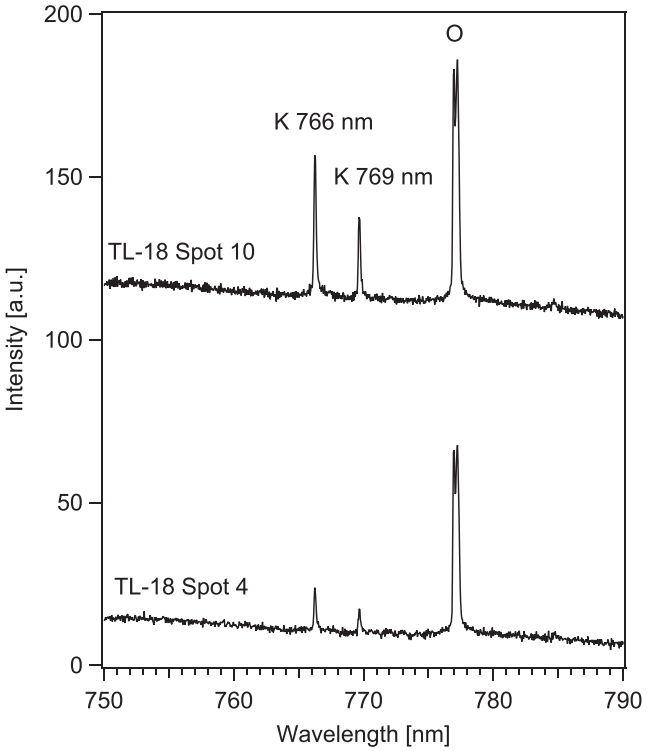

FIGURE 2 LIBS spectra for TL-18 spots #4 and #10 (offset by 100). Two K emission lines are present next to the oxygen triplet peak. Background spectra were subtracted. The instrumental response function is not corrected

The LIBS–MS data obtained in this study are summarized in Table 1. The K_2O–^{40}Ar data pairs follow straight lines[23] very well for both samples (Figure 4). The observed scatter is smaller than those reported in previous studies (e.g., hornblende-biotite gneiss by Cho et al[10]), suggesting a simple cooling history of the basalts supported by their ^{40}Ar–^{39}Ar degassing spectra.[18] Note that the deviation from an isochron could provide background information regarding the sample, such as the degree of disturbance after the rock formation, non-uniformity of trapped ^{40}Ar concentrations, and variation of ages within a rock.[23] Such information provides interpretation of the obtained ages and gives confidence in the age measurement. In these experiments, we did not normalize the abundance of ^{40}K or ^{40}Ar with those of other Ar isotopes, such as ^{36}Ar or ^{38}Ar, because of their low abundances and significant isobaric interferences by hydrocarbons. The measurements of these minor isotopes, however, are not required in our baseline experiments because we assume that trapped ^{40}Ar is uniformly distributed throughout the sample (at the current level of analytical uncertainties) and is addressed by the intercept of the isochron (Figure 4). The use of this K_2O–^{40}Ar isochron may not be valid if the abundance of trapped component is highly heterogeneous within the target rock. In actual missions, supplemental laser ablation to vaporize much larger volume may be used to determine the abundance of these minor isotopes.[1]

The slopes of the isochrons yield 380 ± 44 Ma for TL-18 and 398 ± 50 Ma for TO-35. These ages agree well with the K–Ar ages of the plagioclase grains measured with a conventional technique (i.e., 381 ± 5 Ma for TL-18 and 374 ± 5 Ma for TO-35[18]). Our

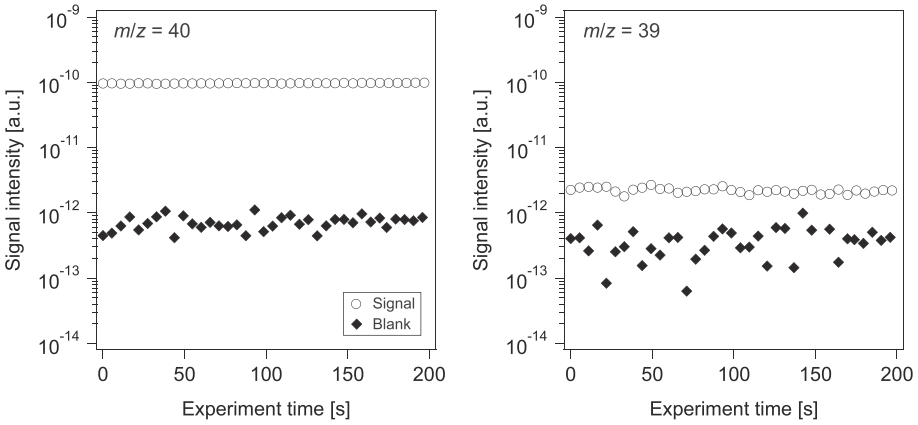

FIGURE 3 Time evolution of gases of selected mass numbers and corresponding blanks for TL-18 spot #10

TABLE 1 Summary of K–Ar data

Sample	Spot	K_2O [wt%]	Mass[a] [μg]	^{40}Ar [10^{-6} cm^3 STP/g]	K–Ar apparent age[b] [Ma]
TL-18	1	0.10 ± 0.10	36 ± 4	1.58 ± 0.49	431 ± 400
	2	0.21 ± 0.10	50 ± 5	2.95 ± 0.43	392 ± 176
	3	0.23 ± 0.10	36 ± 4	5.58 ± 0.84	626 ± 242
	4	0.62 ± 0.10	45 ± 4	12.83 ± 1.65	553 ± 99
	5	0.20 ± 0.10	36 ± 4	2.70 ± 0.43	384 ± 185
	6	0.06 ± 0.10	42 ± 4	2.27 ± 0.35	925 ± 1244
	7	−0.12 ± 0.10	36 ± 4	0.01 ± 0.13	na
	8	0.75 ± 0.10	53 ± 5	9.99 ± 1.25	371 ± 61
	9	0.43 ± 0.10	48 ± 4	13.66 ± 1.74	786 ± 169
	10	2.65 ± 0.28	53 ± 5	44.15 ± 5.31	455 ± 64
	11	1.71 ± 0.13	59 ± 5	23.65 ± 2.79	385 ± 49
	12	0.92 ± 0.10	53 ± 7	12.22 ± 1.85	372 ± 63
	13	1.42 ± 0.13	67 ± 6	14.64 ± 1.70	295 ± 40
TO-35	1	−0.20 ± 0.10	48 ± 4	0.00 ± 0.09	na
	2	0.60 ± 0.10	53 ± 5	11.08 ± 1.36	501 ± 91
	3	0.06 ± 0.10	50 ± 7	2.56 ± 0.43	1058 ± 1456
	4	0.19 ± 0.10	50 ± 7	2.89 ± 0.47	417 ± 204
	5	0.42 ± 0.10	56 ± 7	6.39 ± 0.97	416 ± 104
	6	0.70 ± 0.10	48 ± 7	10.83 ± 1.76	427 ± 82
	7	0.30 ± 0.10	50 ± 7	2.72 ± 0.45	265 ± 93
	8	0.00 ± 0.10	56 ± 9	0.34 ± 0.10	na
	9	−0.07 ± 0.10	53 ± 7	0.20 ± 0.08	na
	10	0.60 ± 0.10	45 ± 6	9.81 ± 1.64	450 ± 94

[a]Density of 2.8 ± 0.2 g/cm^3 was used.

[b]Apparent ages are not calculated for the spots showing zero or negative K concentrations.

experimental results indicate that the current KArLE breadboard achieves a precision of 50 Ma (~12%) for basaltic rocks with a 1σ significance level. The accuracy of the best-fit age was better than 25 Ma, or <7%.

The intercepts of our isochrons indicate that the amount of trapped ^{40}Ar was (11 ± 10) × 10^{-7} cm^3 STP/g for TL-18 and (9 ± 6) × 10^{-7} cm^3 STP/g for TO-35. These values are consistent with the values reported by Ricci et al:[18] 4 × 10^{-7} and 7 × 10^{-7} cm^3 STP/g for TL-18 and TO-35, respectively. If only the bulk rock were measured, the overestimation of age due to the trapped ^{40}Ar of 1.0 × 10^{-6} cm^3 STP would be 61 Ma (an overestimation of 16%) and 290 Ma (76%) when the bulk K_2O contents are 5000 ppm and 1000 ppm, respectively. Furthermore, the intercepts obtained in this study (~1 × 10^{-6} cm^3 STP/g) are lower than previously reported values of 4–15 × 10^{-6} cm^3 STP/g with other rock samples[1,10] and comparable with the amount of bulk-rock excess ^{40}Ar in shergottites (1–2 × 10^{-6} cm^3 STP/g).[24] Our results suggest that the isochron approach enables recognition of trapped ^{40}Ar in situations where it is evenly distributed throughout the mineral phases, such as by incorporation of atmosphere (Mars) or solar wind (moon or asteroids).

The accuracy and precision of an isochron age depend on analytical uncertainties in K–Ar data and the range of K contents.[25] Our experimental results (accuracy <7% and precision <13%) show an improvement in the accuracy and precision of isochron ages compared with previously published results, except for one gneiss sample.[10] In the previous efforts, the relative accuracy for these samples exhibited an overestimation ranging from 0.2 to 33%. The relative precision ranged from 9% for the pyroxene gneiss[10] to 48% for the tuff.[1] Multiple factors contributed to the improvement. First, in terms of the analytical error of individual K–Ar pairs, the median error in $^{40}Ar/K_2O$ ratio was smaller (15%) than those in previous work: 31%[10] and 18%.[1] Second, the range of measured K is larger than found in

some samples in the previous studies, if not all (discussed in the next paragraph). Third, the lack of significant geologic disturbance of the basalt samples could also account for the small scattering of the isochron data, hence the small regression errors. This is in contrast to metamorphic rocks, such as gneiss, which potentially have complicated cooling history and different K–Ar ages within the sample. Fourth, the larger number of data points (N = 13 or 10) also contributes to error reduction compared with most samples measured in the previous studies (N = 6–11). We measured ~10 laser spots in this study to compare our results with those numerically investigated by Bogard.[25] Measuring a large number of laser spots is preferable because the random age error generally decreases according to $(N - 2)^{-1/2}$,[1] while the actual degree of error reduction depends on the distribution of the data points along the isochron. The number of laser spots measured in rover/lander missions would be determined based on various factors, such as whether or not a satisfactory isochron is obtained in the run, the time required for individual age analysis (particularly the time for vacuum pumping), the mobility of the rover/lander, the operational time of the rover/lander, the lifetime of key instruments such as a vacuum pump, the number of interesting samples around the landing site, and the scientific objectives of the entire mission.

The capability to measure a wide range of K is a unique advantage of K–Ar isochron dating by the LIBS–MS approach. Our isochrons show a large spot-to-spot variation of K contents (Figure 4), reflecting the samples' heterogeneity on the scale of the laser spot (three-dimensional parabolic pit with a ~400 μm opening at the sample surface and the depth of ~400 μm). For example, the range of K_2O is larger than ×27 (<1000 ppm–2.7 wt%) for TL-18 and larger than ×7 (<1000–7000 ppm) for TO-35, whereas a fine-grained basalt showed the variation of a factor of 8 (0.29–2.33 wt%) in a previous study.[11] These lines of evidence suggest that a K abundance range larger than a factor of 4, which is used by Bogard[25] as an example of desirable K range, is possible for basaltic samples.

Another advantage of the laser-ablation analysis is its potential to measure small, K-rich phases, which would be diluted by predominantly K-poor phases in a bulk analysis. In fact, the 2.7 wt% K_2O for TL-18 is more than twice as high as its bulk K_2O concentration of 1.1 wt% and > 6 times higher than that of plagioclase in this sample (4200 ppm).[18] This is probably because the laser spot sampled a K-rich phase, such as glass in the groundmass. Our data show no evidence of K or Ar loss from this high-K phase. The direct measurement of such a K-rich phase by spot-by-spot analysis would be particularly useful for measuring samples with very low bulk K concentration (K_2O <1000 ppm) containing small, K-rich phases, such as shergottites.[24]

The highest K abundances in the TO-35 isochron was 6000–7000 ppm. This abundance is consistent with the K content of plagioclase in the sample (6400 ppm)[18] and is the lowest K maximum content in the isochrons obtained with the LIBS–MS approach. Our results suggest that the isochron measurement yields accurate and precise ages for a sample where plagioclase is the dominant K-bearing phase, significantly expanding the applicability of this approach to more K-poor rocks. Obtaining an accurate and precise isochron with the maximum K_2O of 7000 ± 1000 ppm is particularly important because this result suggests that very K-rich phases, such as biotite or K-feldspar in the gneiss samples, are not required for LIBS–MS measurements.

Because only a small amount of sample is vaporized by laser ablation, accurately measuring the amount of ^{40}Ar has been one of the challenges of the LIBS–MS approach. The ^{40}Ar concentrations measured in this study were of the order of 10^{-6} to 10^{-5} cm^3 STP/g depending on the K content of individual spots (Table 1). The highest ^{40}Ar contents here are 10–30 times lower than those measured by previous studies.[1,10] This result experimentally shows that the quadrupole mass spectrometer yields ^{40}Ar amounts accurately at this abundance range, demonstrating that K–Ar ages are measurable from these ^{40}Ar-poor rocks. Another advantage to this low detection limit of ^{40}Ar is in reducing the required sample mass to liberate a given amount of ^{40}Ar, which could enhance the spatial resolution of LIBS–MS analysis, or reduce the number of laser shots required per sample spot. Reducing the number of laser shots would reduce the time required for onboard experiments and the power consumption of the laser.

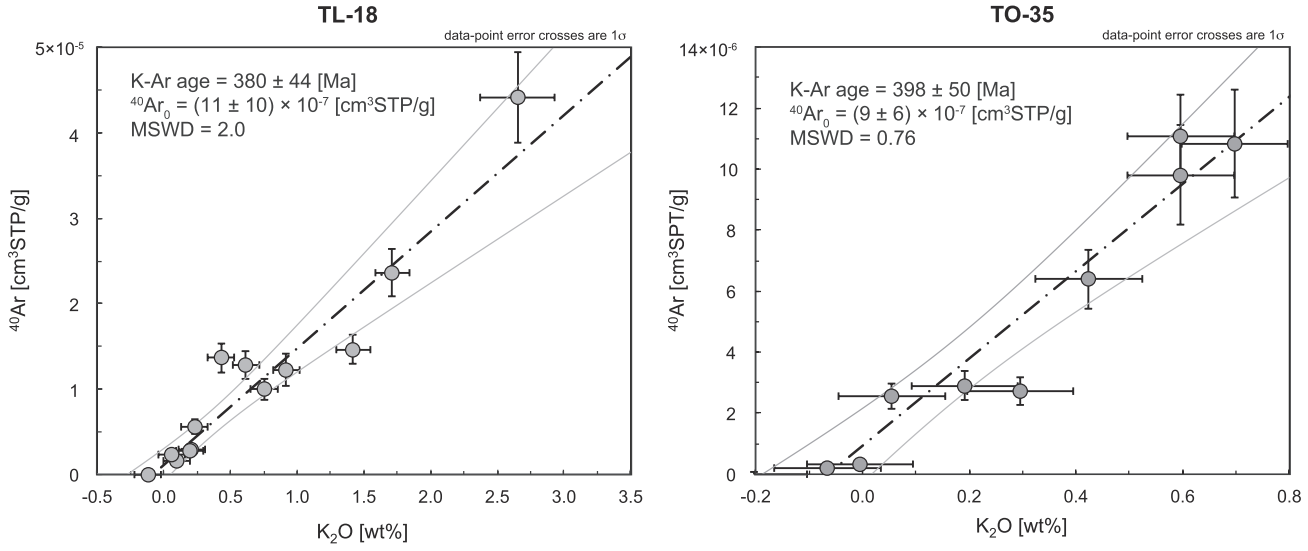

FIGURE 4 K–Ar isochrons for two basaltic samples. The dashed lines indicate the best-fit isochrons

The volume of the 23 laser pits measured in this study was (1.8 ± 0.3) × 10^7 μm^3, which is equivalent to 49 ± 8 μg. A weak positive correlation (R = 0.7) was observed between the K content and ablation volume with TL-18, whereas no correlation was found with TO-35. The larger mineral size of TL-18 could account for the different ablation efficiency of different mineral species. The observed sample mass is comparable with those reported by Cohen et al[1] (~50 μg) and between those reported by Devismes et al[11] (~14 μg) and Cho et al[10] (~100 μg). The volume differences with the latter two studies can be attributed to pulse numbers (i.e., 500 in this study vs 300[11]), spot diameters (i.e., 400 μm in this study vs 250 μm[11]), different laser wavelengths (i.e., 1064 nm in this study vs 266 nm[11]), different laser pulse energies (i.e., 30 mJ in this study vs 100 mJ[10]), or the relative hardness of the materials, where softer rocks develop deeper and larger-diameter pits for the same laser energy deposited.[1]

The isochron plots in this study used the K–Ar data pairs of all the spots measured in the experiments. This is in contrast to Cho et al,[10] where a few isochron data were excluded based on the following reasons. The first reason involved variation of the K abundance within a laser spot. Because of the three-dimensional distribution of minerals, the concentration of K could vary in the depth direction as laser ablation proceeds. Our data, however, did not show any significant change in K content as the laser pulses excavated the samples. This is probably because the laser pits in this study were smaller than those of Cho et al,[10] so only a single mineral phase was interrogated each time. Note that heterogeneous K measurements can be accommodated by assigning a bulk K measurement to the pit material based on the LIBS spectra with depth. The second reason for the data selection involved spallation during development of laser pits, which may make the volume measurements unreliable. No laser pit, however, exhibited fragmentation in this study. This may be because the pulse energy used in this study (30 mJ) is much lower than that of Cho et al[10] (100 mJ). Another plausible explanation is that the laser–sample coupling was good for these basaltic rocks. The issue of spallation can be addressed by better understanding laser pit development in multiple geologically relevant samples, including the relationships between laser energy, number of pulses, and pit depth.[26] The overall results show that the LIBS–MS approach works without noticeable issues even with the 30-mJ laser and without a cold trap or a high-temperature getter, strongly suggesting that the LIBS–MS approach can be implemented with flight-proven instruments.

We also found that the isochron approach is robust against the isobaric interferences by hydrocarbons from the samples. Isochron fitting for the data before the isobaric correction yielded the ages consistent with the known ages within 1σ error: 356 ± 46 Ma for TL-18 and 398 ± 51 Ma for TO-35. This is because the concentration of the hydrocarbon can be deemed constant and/or insignificant over every spot measurement. The contribution of C_3H_4 to the total signal at m/z 40 (C_3H_4/(^{40}Ar + C_3H_4)) varied from 0.01 (for ^{40}Ar-rich spots) to 1 (for the spots used to quantify C_3H_4 abundances). The median of this ratio was 0.09 and 0.17 for TL-18 and TO-35, respectively. In fact, the lack of the correction would just increase the intercept of the isochron by a factor of 2, to 2.9 × 10^{-6} (TL-18) and 1.6 × 10^{-6} (TO-35) cm^3 STP/g, but would not change the isochron slopes significantly. This is a good contrast with the model age approach, in which incomplete isobaric correction directly increases age values. This robustness is advantageous for obtaining accurate age values under the presence of hydrocarbons or chlorinated compounds, which is typical on Mars.[27,28]

The laser-ablation approach yields multiple age data from a single sample by measuring multiple spots. In addition to the isochron ages, therefore, we can calculate spot-by-spot apparent ages based on the K–Ar pairs from individual laser spots (Table 1) to investigate the accuracy and precision of the spot-by-spot dating (Figure 5). Determining spot-by-spot ages is useful for examining the performance of the LIBS–MS approach for various K concentrations without measuring a number of different rocks. The ages of individual spots were determined after the isobaric correction. Because calculating the apparent ages is equivalent to determining the slope of each data point in Figure 4 by assuming that the y-intercept is exactly zero, the apparent K–Ar ages deviate from the isochron age if a trapped or lost component is present. First, the weighted averages of the overall apparent K–Ar ages are calculated to compare the apparent ages with the isochron ages. Weighting was implemented to address the large errors associated with low-K data. We thus obtained 380 ± 22 Ma for TL-18 and 414 ± 40 Ma for TO-35. While the results from TL-18 show a strikingly accurate and precise age, those from TO-35 indicate a broad

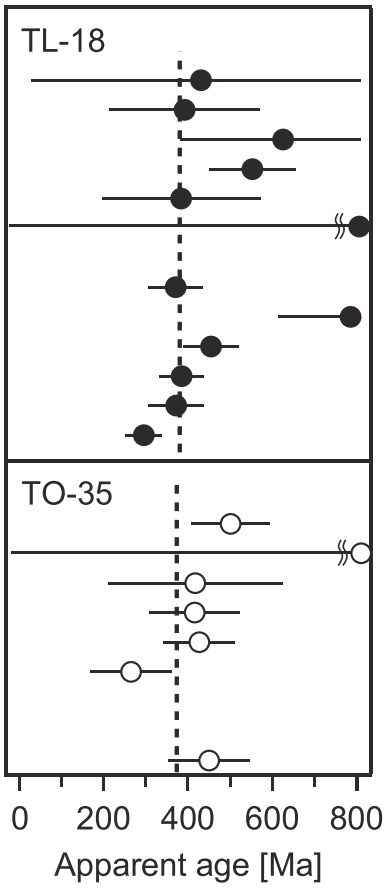

FIGURE 5 Apparent K–Ar ages for individual laser spots. TL-18 spot #1 to TO-35 spot #10 to from the top to the bottom. Vertical dashed lines indicate the published K–Ar ages of each sample. Negative apparent ages (spot #7 of TL-18, spots #1, 8, and 9 of TO-35) are not shown. Two samples with >1000 Ma with large error bars are shown with wavy lines

overestimation, at least partly due to trapped ^{40}Ar. This overestimation underlines the importance of isochron analysis particularly when the K abundance is low or the sample is young.

Second, the accuracy and precision of the $[^{40}Ar]/[K_2O]$ ratios obtained in this study are shown as a function of K abundance since potassium abundance is a fundamental parameter for K–Ar dating (Figure 6). General improvements in accuracy and precision with an increase in K_2O are observed. The median accuracy and precision of nine spots having K_2O content higher than 5000 ppm were 14% and 22%, respectively, after correcting for isobaric interference and trapped Ar. This level of analytical error results in an accuracy of ±48 Ma and a precision of ±75 Ma for a 380-Ma rock. On the other hand, the median relative accuracy and precision of our six $^{40}Ar/K_2O$ data exhibiting K_2O between 1000 and 3000 ppm were 41% and 70%, respectively. Figure 6 also indicates that the overall accuracy improved after the isobaric and trapped corrections, particularly in the low-K range (< ~3000 ppm). This is because the relative contribution of the trapped ^{40}Ar is larger for the K-poor (and therefore Ar-poor) spots. Some data in our experiments show negative ages. Our LIBS calibration yields negative K contents when $I_K/I_{total} < 0.00089$ (Figure 1). Neither these K contents nor the resulting age values are reliable, but measuring such K-poor spots is essential for estimating the concentration of the trapped component. This ability is a unique advantage of the LIBS–MS method.

Multiple error sources contribute to the final age determination errors (Equation 2). Potassium abundance was the largest error source except for spots #11 and #12 of TL-18. The errors in sample density ρ (7%), laser pit volume V (5–15%; median = 8%), and ^{40}Ar amount (8–36% excluding the spots used for the C_3H_4/C_3H_3 ratio assessments; median = 9%) were similar.

In our breadboard, the uncertainty in K_2O abundance above the detection limit ranged from 8% to 99% depending on the K_2O content, with a median of 17%. Several improvements could be made to improve this uncertainty. A previous LIBS study using a high-sensitivity optical spectrometer, which has a quantum efficiency comparable with that of the ChemCam, showed that the K measurement error is much improved, particularly for low-K samples. The errors were estimated as ±400 ppm at 1000 ppm K_2O; ±600 ppm at 3000 ppm; and ±900 ppm at 5000 ppm.[6] If a 4000 Ma rock with 3000 ppm K_2O is measured, for example, a K_2O error reduction from ±1000 ppm to ±600 ppm decreases the age error by 200 Ma. The use of an intensified CCD (ICCD) detector, which is planned for the SuperCam instrument,[29] could also lead to higher precision. Stipe et al[30] reported an error of ±8% at 6100 ppm K_2O using an ICCD camera as a detector. Furthermore, measuring the full range of elemental abundances and using the partial least squares (PLS) regression could improve the accuracy of K_2O abundances.[31,32] The use of sub-model training sets, which are composed of calibration samples having a more relevant concentration range, was shown to improve measurement capabilities.[31] Therefore, training the PLS model using a number of low-K (hundreds to thousands of ppm) standards would be particularly useful to enable accurate analysis of K in this concentration range.

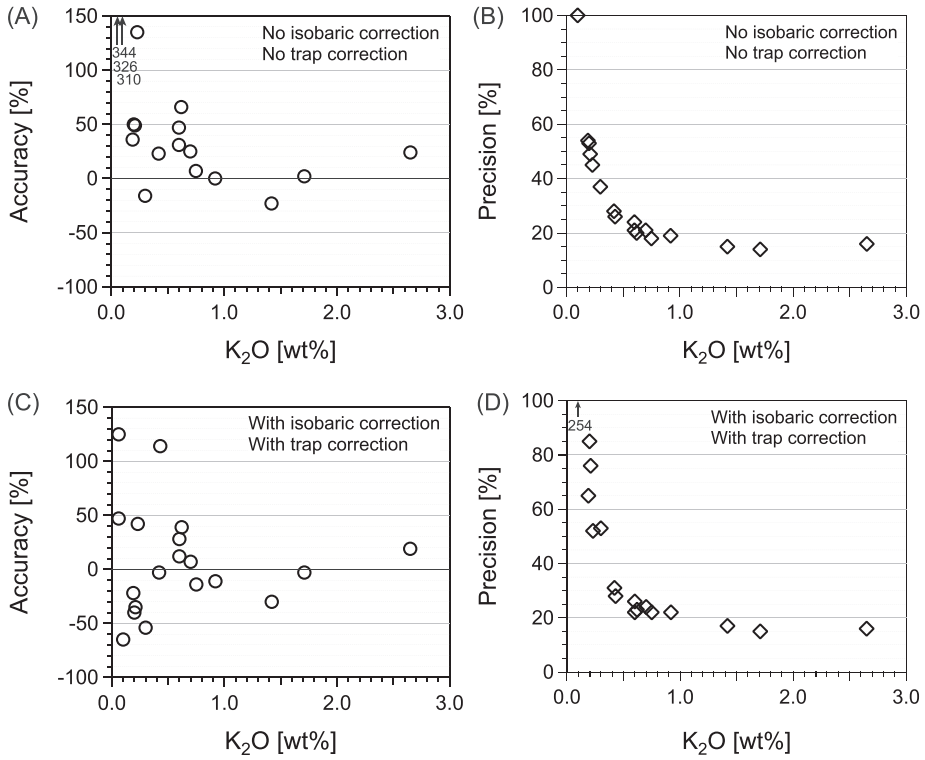

FIGURE 6 Relative accuracy and precision of $^{40}Ar/K_2O$ ratios measured at individual laser spots before trapped Ar or isobaric species corrections (A, B) and after trapped Ar and isobaric species correction (C, D). Positive accuracy means an overestimation; zero accuracy means exactly accurate. General improvements in accuracy and precision with an increase in K_2O are observed as expected. Three data points in (A) fall beyond 150% and they are shown by their numbers (600 ppm, 344%; 600 ppm, 326%, and 1000 ppm, 310%)

TABLE 2 Source of uncertainties and potential improvements to achieve target error values

	Method	Dominant sources of uncertainty in breadboard	Potential improvements for flight	Error budget
K	LIBS	Low signal-to-noise ratio for K lines, calibration for low-K samples	Better calibration set, PLS data reduction, high-QE detector	10%
Ar	Mass spectrometry	Uncertainty in mass spectrometer sensitivity, high blank levels	Precise determination of mass spectrometer sensitivity, smaller manifold volume (higher partial pressure)	5%
Volume	Optical metrology	Vertical resolution of volume reconstruction	Higher-resolution imaging	10%
Density	Computed	Mineralogy, porosity	PLS data reduction, higher-resolution imaging	5%
RSS error				16%

For the ^{40}Ar measurements, the largest contributor to the age error in our breadboard configuration is the sensitivity of the mass spectrometer α (relative precision of 8%); other terms in Equation 2, such as the regression errors of signals and blanks at m/z 40 and 39, blank corrections at m/z 40 and 39, or the isobaric correction, made only minor contributions to the uncertainty. For flight instruments, the sensitivity is extremely well characterized,[2] so we do not expect this to be a large contributor in the flight version of the system. Another difference between our laboratory setup and a flight instrument is in the volume of the vacuum line. Flight mass spectrometers use much smaller manifolds, resulting in higher partial pressure of gases for a given abundance. Therefore, the uncertainty associated with signal intensities is expected to be much smaller, leading to more accurate and precise measurement of blank mass spectra. This will also reduce the error involved with the blank and isobaric corrections and allow us to determine ^{40}Ar abundance with smaller uncertainties.

The capability of KArLE can be predicted from our experimental results, potential improvements, and limitations of flight instruments. Table 2 summarizes the parameters determining K–Ar ages, the dominant sources of uncertainties, potential approaches to improving them, and the error budget for each measurement to achieve an uncertainty of ±100 Ma on a 4000 Ma planetary sample. To meet this age uncertainty, the root sum square (RSS) error in each laser spot must be 16% or less and an isochron must be constructed consisting of eight or more spots. The error allocation for ^{40}Ar is currently achievable with flight instruments: geochronology experiments using SAM achieved 3–5% errors in ^{40}Ar.[2,3] These experiments estimated the sample mass using spacecraft parameters, but an alternative approach to mass determination using sample density ρ and laser pit volume V is estimated to be achievable with 5% and 10% uncertainties using flight-like imaging resolution.[1] A precision of ±3200 ppm has been reported for K using ChemCam[31] and a feasibility study for future lunar missions showed that precision of ±1600 ppm is possible.[33] By reducing LIBS errors on K abundance to 10% and measuring eight meaningful laser spots for isochron analysis, we would achieve a ±100 Ma error for 4000 Ma rocks.

The age error estimations suggest that *in situ* K–Ar geochronology with our LIBS–MS approach would be able to resolve a wide range of issues in planetary science. For example, the LIBS–MS geochronology would determine the absolute ages of a variety of geologic units explored by Mars rovers/landers. Such measurements will provide key data to improve our understandings on the changing habitability of ancient Mars: anchoring the absolute timing of the transition between Noachian and Hesperian. The Hesperian–Amazonian transition, which has a two-billion-years uncertainty in the middle part of the Martian chronology,[34] would be determined much more accurately and precisely. For *in situ* geochronology on the Moon, the measurement error would be sufficiently small to determine the age of key lunar basins where crater counting saturates,[35,36] and constrain the impact flux at the 1000–3000 Ma range, where the crater chronology models may have an uncertainty up to ±1000 Ma.[37]

4 | CONCLUSIONS

The state-of-the-art capability of *in situ* K–Ar geochronology is examined based on the case study for two ~380 Ma basaltic rocks. The LIBS–MS instrument was updated to improve the fidelity to the flight-equivalent experimental devices in terms of laser energy or a cold trap. Both samples exhibit well-defined isochron plots. The isochron slopes yield ages of 380 ± 44 Ma and 398 ± 50 Ma for 380.7-Ma and 373.5-Ma rocks, respectively, experimentally indicating that accuracy better than 25 Ma (<7%) and precision of ±50 Ma (13%) are achievable with our current breadboard. The intercepts of the isochrons both yielded the amount of trapped ^{40}Ar as approximately 1×10^{-6} cm^3 STP/g, which is comparable with the amount of excess ^{40}Ar found in shergottites. The ranges of K_2O were < 1000–7000 ppm or < 1000 ppm–2.7 wt%. The maximum K contents of these isochron plots are a factor of two to one order of magnitude lower than those measured with previous studies. This result validates the capability of measuring K-poor rocks, where plagioclase is the main K-bearing phase. The noble gas analysis using the mass spectrometer yielded ^{40}Ar concentrations of approximately 10^{-6} to 10^{-5} cm^3 STP/g, one order of magnitude lower than those obtained by previous studies. This result indicates that KArLE can measure K-poor and/or young rocks, as well as the gas released from much smaller sample volumes. The capability of reducing sample mass leads to fewer laser pulses being necessary and higher spatial resolution of analyses, both of which are advantageous for *in situ* measurements. Our experimental results demonstrate that accurate and precise measurements are possible using the KArLE approach on basaltic rocks, which are ubiquitous on planetary surfaces. This capability is useful in addressing a wide range of questions in planetary science.

ACKNOWLEDGEMENTS

We thank Dr. Fanny Cattani and her colleagues for providing the basaltic samples. We thank Ms. Midori Oguma for preprocessing the LIBS data. Y. Cho was supported by funds from the Japan Society for the Promotion of Science (JSPS) Postdoctoral Fellowship for Research Abroad. We would like to acknowledge the appraisal by the Editor Prof. J. Monaghan, the careful and constructive reviews by Prof. J. Solé, and two anonymous reviewers for improving this manuscript.

ORCID

Yuichiro Cho http://orcid.org/0000-0003-2749-2204

REFERENCES

1. Cohen BA, Miller JS, Li Z-H, Swindle TD, French RA. The Potassium-Argon Laser Experiment (KArLE): in situ geochronology for planetary robotic missions. *Geostand Geoanal Res*. 2014;38(4):421-439. https://doi.org/10.1111/j.1751-908X.2014.00319.x
2. Farley KA, Malespin C, Mahaffy P, et al. In situ radiometric and exposure age dating of the Martian surface. *Science*. 2014;343. 1247166-1-5. https://doi.org/10.1126/science.1247166
3. Martin PE, Farley KE, Baker MB, et al. A two-step K-Ar experiment on Mars: Dating the diagenetic formation of jarosite from Amazonian groundwaters. *J Geophys Res Planets*. 2017;122(12):2803-2818. https://doi.org/10.1002/2017JE005445
4. Vasconcelos PM, Farley KA, Malespin CA, et al. Discordant K-Ar and young exposure dates for the Windjana sandstone, Kimberley, Gale Crater. *Mars J Geophys Res Planets*. 2016;121(10):2176-2192. https://doi.org/10.1002/2016je005017
5. Cattani F, Gillot P-Y, Devismes D, et al. Checking, with a set of terrestrial analogue rock minerals, a system for possible in-situ K-Ar dating at the surface of Mars. *Lunar Planet Sci*. 2017;48:1864.
6. Cho Y, Horiuchi M, Shibasaki K, Kameda S, Sugita S. Quantitative potassium measurements with laser-induced breakdown spectroscopy using low-energy lasers: application to in situ K-Ar geochronology for planetary exploration. *Appl Spectrosc*. 2017;71(8):1969-1981. https://doi.org/10.1177/0003702817701941
7. Cho Y, Kameda S, Miura YN, et al. Conceptual design of an in situ K-Ar isochron dating instrument for future Mars rover missions. *Trans JSASS, Aerospace Tech Japan*. 2016;14(ists30):Pk_89-Pk_94. https://doi.org/10.2322/tastj.14.Pk_89
8. Cho Y, Kameda S, Okuno M, et al. Experimental characterization of elastomeric O-rings as reusable seals for mass spectrometric measurements: Application to in situ K–Ar dating on Mars. *Adv Space Res*. 2017;60:1453-1462. https://doi.org/10.1016/j.asr.2017.07.002
9. Cho Y, Sugita S, Kameda S, et al. High-precision potassium measurements using laser-induced breakdown spectroscopy under high vacuum conditions for in situ K–Ar dating of planetary surfaces. *Spectrochim Acta B*. 2015;106:28-35. https://doi.org/10.1016/j.sab.2015.02.002
10. Cho Y, Sugita S, Miura YN, Okazaki R, Morota T, Kameda S. An in-situ K-Ar isochron dating method for planetary landers using laser-ablation technique. *Planet Space Sci*. 2016;128:14-29. https://doi.org/10.1016/j.pss.2016.05.004
11. Devismes D, Gillot P-Y, Lefèvre J-C, Boukari C, Rocard F, Chiavassa F. KArMars: A breadboard model for in situ absolute geochronology based on the K-Ar method using UV-laser induced breakdown spectroscopy and quadrupole mass spectrometry. *Geostand Geoanal Res*. 2016;40(4):517-532. https://doi.org/10.1111/ggr.12118
12. Solé J. In situ determination of K–Ar ages from minerals and rocks using simultaneous laser-induced plasma spectroscopy and noble gas mass spectrometry. *Chem Geol*. 2014;388:9-22. https://doi.org/10.1016/j.chemgeo.2014.08.027
13. Ehlmann BL, Edwards CS. Mineralogy of the Martian surface. *Annu Rev Earth Planet Sci*. 2014;42(1):291-315. https://doi.org/10.1146/annurev-earth-060313-055024
14. Nimmo F, Tanaka K. Early crustal evolution of Mars. *Annu Rev Earth Planet Sci*. 2005;33:133-161. https://doi.org/10.1146/annurev.earth.33.092203.122637
15. Maurice S, Clegg SM, Wiens RC, et al. ChemCam activities and discoveries during the nominal mission of the Mars Science Laboratory in Gale crater. *Mars J Anal At Spectrom*. 2016;31(4):863-889. https://doi.org/10.1039/c5ja00417a
16. Maurice S, Wiens RC, Saccoccio M, et al. The ChemCam Instrument Suite on the Mars Science Laboratory (MSL) Rover: Science objectives and mast unit description. *Space Sci Rev*. 2012;170(1):95-166. https://doi.org/10.1007/s11214-012-9912-2
17. De Giacomo A. Experimental characterization of metallic titanium-laser induced plasma by time and space resolved optical emission spectroscopy. *Spectrochim Acta B*. 2003;58:71-83.
18. Ricci J, Quidelleur X, Pavlov V, Orlov S, Shatsillo A, Courtillot V. New $^{40}Ar/^{39}Ar$ and K–Ar ages of the Viluy traps (Eastern Siberia): Further evidence for a relationship with the Frasnian–Famennian mass extinction. *Palaeogeogr Palaeoclimatol Palaeoecol*. 2013;386:531-540. https://doi.org/10.1016/j.palaeo.2013.06.020
19. Corsi M, Cristoforetti G, Hidalgo M, et al. Effect of laser-induced crater depth in laser-induced breakdown spectroscopy emission features. *Appl Spectrosc*. 2005;59:853-860.
20. Bredice F, Borges FO, Sobral H, et al. Evaluation of self-absorption of manganese emission lines in laser induced breakdown spectroscopy measurements. *Spectrochim Acta B*. 2006;61(12):1294-1303. https://doi.org/10.1016/j.sab.2006.10.015
21. Wiens R, Maurice S, Barraclough B, et al. The ChemCam instrument suite on the Mars Science Laboratory (MSL) rover: body unit and combined system tests. *Space Sci Rev*. 2012;170(1):167-227. https://doi.org/10.1007/s11214-012-9902-4
22. Lee J-Y, Marti K, Severinghaus JP, et al. A redetermination of the isotopic abundances of atmospheric Ar. *Geochim Cosmochim Acta*. 2006;70(17):4507-4512. https://doi.org/10.1016/j.gca.2006.06.1563
23. Harper CT. Graphical solutions to the problem of radiogenic Ar-40 loss from metamorphic minerals. *Eclogae gelo Helv*. 1970;63(1):119-140.
24. Bogard D, Park J, Garrison D. ^{39}Ar-^{40}Ar "ages" and origin of excess ^{40}Ar in Martian shergottites. *Meteorit Planet Sci*. 2009;44(6):905-923.
25. Bogard DD. K-Ar dating of rocks on Mars: Requirements from Martian meteorite analyses and isochron modeling. *Meteorit Planet Sci*. 2009;44(1):3-14.
26. Devismes D, Cohen BA. Continued development of in situ geochronology for planetary using KArLE (Potassium-Argon Laser Experiment). *Lunar Planet Sci*. 2016;47:2046.
27. Ming DW, Archer PD, Glavin DP, et al. Volatile and organic compositions of sedimentary rocks in Yellowknife Bay, Gale crater. *Mars Science*. 2014;343(6169). 1245267-1-9. https://doi.org/10.1126/science.1245267
28. Freissinet C, Glavin DP, Mahaffy PR, et al. Organic molecules in the Sheepbed Mudstone, Gale Crater. *Mars J Geophys Res Planets*. 2015;120:495-514. https://doi.org/10.1002/2014JE004737
29. Wiens RC, Maurice S, McCabe K, et al. The SuperCam remote sensing instrument suite for Mars 2020. *Lunar Planet Sci*. 2016;47:1322.
30. Stipe CB, Guevara E, Brown J, Rossman GR. Quantitative laser-induced breakdown spectroscopy of potassium for in-situ geochronology on Mars. *Spectrochim Acta B*. 2012;70:45-50. https://doi.org/10.1016/j.sab.2012.04.010
31. Anderson RB, Clegg SM, Frydenvang J, et al. Improved accuracy in quantitative laser-induced breakdown spectroscopy using sub-models. *Spectrochim Acta B*. 2017;129:49-57. https://doi.org/10.1016/j.sab.2016.12.002
32. Dyar MD, Fassett CI, Giguere S, et al. Comparison of univariate and multivariate models for prediction of major and minor elements from laser-induced breakdown spectra with and without masking. *Spectrochim Acta B*. 2016;123:93-104. https://doi.org/10.1016/j.sab.2016.07.010

33. Lasue J, Wiens RC, Clegg SM, et al. Remote laser-induced breakdown spectroscopy (LIBS) for lunar exploration. *J Geophys Res Planets*. 2012;117:E01002. https://doi.org/10.1029/2011je003898

34. Doran P, Clifford SM, Forman SL, et al. Mars chronology: assessing techniques for quantifying surficial processes. *Earth Sci Rev*. 2004;67(3–4):313-337. https://doi.org/10.1016/j.earscirev.2004.04.001

35. Bottke WF, Norman MD. The late heavy bombardment. *Annu Rev Earth Planet Sci*. 2017;45:619-647. https://doi.org/10.1146/annurev-earth-063016-020131

36. Cohen BA. The onset of the cataclysm: in situ dating of the Nectaris basin impact melt sheet. Annual Meeting of the Lunar Exploration Analysis Group 2017;5051.

37. Robbins SJ. New crater calibrations for the lunar crater-age chronology. *Earth Planet Sci Lett*. 2014;403:188-198. https://doi.org/10.1016/j.epsl.2014.06.038

How to cite this article: Cho Y, Cohen BA. Dating igneous rocks using the Potassium–Argon Laser Experiment (KArLE) instrument: A case study for ~380 Ma basaltic rocks. *Rapid Commun Mass Spectrom*. 2018;32:1755–1765. https://doi.org/10.1002/rcm.8214